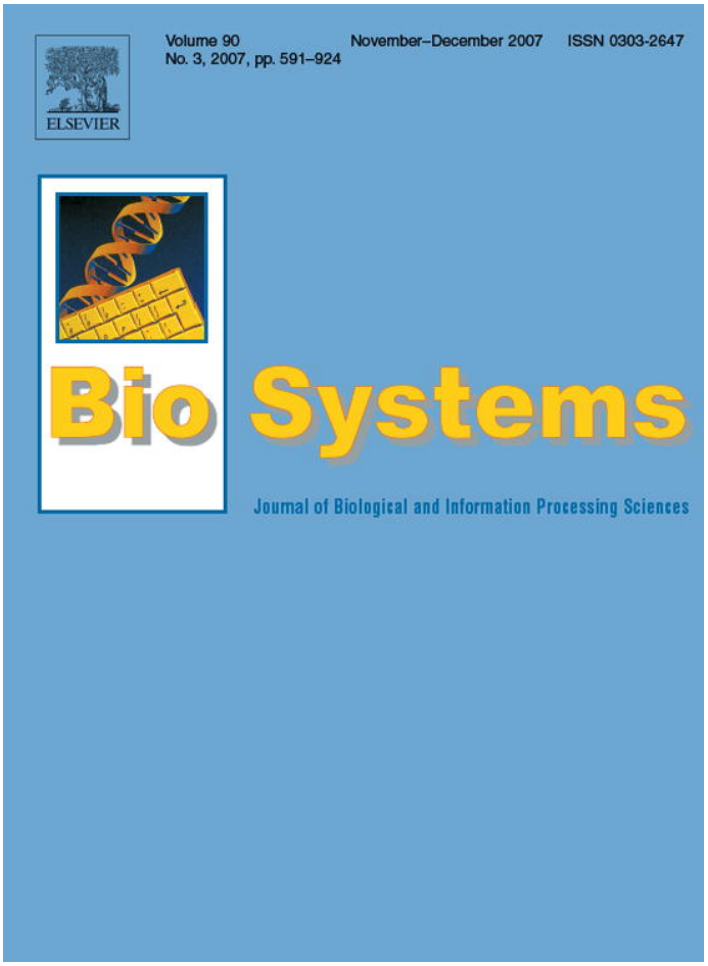

Available online at www.sciencedirect.com
ScienceDirect
BioSystems 90 (2007) 750–768
BioSystems
www.elsevier.com/locate/biosystems

A neurobiological model of the recovery strategies from perturbed walking

Sungho Jo

Biomechatronics Group, Media Laboratory, Massachusetts Institute of Technology, 20 Ames St. E15-054, Cambridge, MA 02139, USA

Received 7 December 2006; received in revised form 23 March 2007; accepted 26 March 2007

Abstract

This paper proposes a human mimetic neuro-musculo-skeletal model to simulate the recovery reactions from perturbations during walking. The computational model incorporates nonlinear viscoelastic muscular mechanics, supraspinal control of the center-of-mass, spinal pattern generator including muscle synergy network, spinal reflexes, and long-loop reflexes. Especially the long-loop reflexes specify recovery strategies based on the experimental observations [Schillings, A.M., van Wezel, B.M.H., Mulder, T.H., Duysen, J., 2000. Muscular responses and movement strategies during stumbling over obstacles. J. Neurophysiol. 83, 2093–2102; Eng, J.J., Winter, D.A., Patla, A.E., 1994. Strategies for recovery from a trip in early and late swing during human walking. Exp. Brain Res. 102, 339–349]. The model demonstrates two typical recovery strategies, i.e., elevating and lowering strategies against pulling over a swing leg. Sensed perturbation triggers a simple tonic pulse from the cortex. Depending on the swing phase, the tonic pulse activates a different compound of muscles over lower limbs. The compound induces corresponding recovery strategies. The reproduction of principal recovery behaviors may support the model's proposed functional and/or anatomical correspondence.

Keywords: Bipedal walking model; Cerebrocerebellar feedback system; Spinal pattern generator; Recovery strategies; Perturbed walking; Long-loop feedback

1. Introduction

A computational model of cerebrocerebellar and spinomuscular interactions in the control of bipedal walking in the sagittal plane has been proposed in previous studies (Jo and Massaquoi, 2007). The model actuates a six joint rigid body by the muscular dynamics which receives the neural command from the supraspinal long-loop feedback system, the spinal locomotive pattern generator, and the segmental reflexes. The model achieved stable sagittal planar walking simulations under the effect of neural delays, and demonstrated the recovery of steady walking against varied amounts of impulsive pushes and proposed a scheme of changing walking speeds. In the model, the supraspinal long-loop feedback system mainly manages postural balance while the spinal pattern generator with segmental reflexes executes gaits. The purposes of developing the model were to find almost minimal requirement of the sensorimotor neural systems for nominal gaits while an integrated model includes each neural system model explicitly and to propose a neurobiological mechanism principle of gaits. Since the model was originally designed to simulate normal human walking, further improvement of the model is required for generation of realistically perturbed walking. This paper studies computationally the recovery behaviors of walking after perturbed using an augmented neuro-musculo-skeletal model.

E-mail address: shjo@media.mit.edu.

0303-2647/$ – see front matter © 2007 Elsevier Ireland Ltd. All rights reserved.
doi:10.1016/j.biosystems.2007.03.003

Human recovery reactions during gaits have been experimentally investigated in the past from various perspectives (Schillings et al., 2000; Cordero et al., 2003, 2004; Zehr and Stein, 1999; Eng et al., 1994). In experiments by Cordero et al. (2003), the lower leg is pulled backward shortly while a subject walks normally. The perturbation is applied in either the early or late swing phase. In the early swing phase, duration of the perturbation lasts a long or short period of time, and in the late swing phase, it lasts a short period. Typical human response demonstrates two recovery strategies: "elevating strategy", and "lowering strategy" (Cordero et al., 2003, 2004). The recovery behaviors can be classified in terms of step length and step time. Elevation strategy maintains at least normal step length with normal step time. Therefore, the flexion angles of joints of the swinging leg increase after perturbation. However, the lowering strategy shortens step length because the foot of the swinging leg is rapidly lowered to the ground. Therefore, joint excursions, especially in the swinging hip joints, are smaller. Both reactions require multiple-step process for recovery. It is experimentally observed that people usually use an elevation strategy when perturbed in the early swing phase, and a lowering strategy when perturbed in the late swing phase (Cordero et al., 2003, 2004; Schillings et al., 2000). Therefore, the recovery strategies depend on the gait phase. The two typical recovery strategies are originally named from stumbling behaviors over obstacles during treadmill walking (Eng et al., 1994; Schillings et al., 2000).

Schillings et al. (2000) measured muscular responses while stumbling over obstacles. A swing leg was perturbed by an obstacle during gaits on the treadmill. They suggested that the functionally important recovery strategies are performed by muscular responses at latencies from 60 to 140 ms. The latency timing may indicate that long-loop reflexes through the cortex supervise the phase-dependent selection of the recovery strategy. Moreover, similar observations have suggested that a transcortical reflex pathway contributes to cutaneous reflexes in the tibialis anterior muscle in human walking (Christensen et al., 1999; Nielsen, 2003).

2. Methods

2.1. Principal assumptions for modeling

In this paper, it is assumed that long-loop reflexes through the cortex are necessary to carry out different functional recovery strategies corresponding to experimental observations of muscular responses with long latencies (Schillings et al., 2000; Eng et al., 1994). Different muscular activations by the long-loop reflexes evoke different recovery behaviors. In addition, selecting the different recovery strategies is phase-dependent. In the model, the phase is described by sensing of the body states.

When a perturbation is applied, a cutaneous receptor detects the perturbation, and the detection is subsequently informed to the cortex (Christensen et al., 1999; Pijnappels et al., 1998; Eng et al., 1994). Depending on the phase when the perturbation evokes, the cortex descends a neural pulse to a different muscle group. For perturbation in the early swing phase, the neural pulse assumes to activate the flexors in the swing leg resulting in larger joint excursion, thus indicating the elevating strategy. For perturbation in the late swing phase, the descending neural pulse is assumed to activate hip and knee flexors and plantarflexor at the ankle in the swing leg. An interesting point is that plantarflexor (especially, Soleus) is rigorously active in the lowering strategy, and dorsiflexor (especially, Tibialis anterior) is relatively rigorously in the elevating strategy (Schillings et al., 2000). From the mechanical viewpoint, the plantarflexor activation in the lowering strategy may be helpful to keep the body's center-of-mass (COM) within a feasible supporting area because the COM is moving forward due to the perturbation. On the other hand, the dorsiflexor activation in the elevating strategy is probably to drive swing excursion by lifting the foot up. In either perturbation, it is assumed that the descending neural pulse also activates hip extensor and knee flexor muscles of the stance leg. This helps support the upper body while the swing leg executes a strategic behavior. For this computational study, the muscular activations in the model are implemented to mimic the muscular activation patterns observed from experimental studies (Schillings et al., 2000; Pijnappels et al., 2004; Eng et al., 1994). However, not every muscular activation from human experiments was provided. Therefore, they are empirically tuned to obtain realistic recovery behaviors. An important modeling assumption is that the long-loop reflex is a major determinant of the elevating strategy. On the other hand, spinal reflexes modulate the lowering strategy influentially against a reasonable magnitude of perturbation. In the late swing perturbation, a short time interval exists between the perturbation application and the ground touch for the long-loop reflex to operate effectively. Therefore, spinal reflexes may be sufficient to not fall. However, the long-loop reflex can still be helpful to a sequential recovery after the perturbation because recovery is generally not achieved in a single step but in multiple steps (Cordero et al., 2003). Furthermore, spinal reflexes alone would not be able to maintain stable walking posture without the long-loop reflex against a large perturbation in the late swing phase. The long-loop reflex may still be effective for robust recovery.

A neural mechanism of selecting the recovery strategy needs to be modeled. However, the neural mechanism of the selection in human still remains neurophysiologically unexplored. This paper proposes a possible switching mechanism for the selection. From the proprioceptive information of the swing leg (see Section 2.2.5.2), the supraspinal system esti-

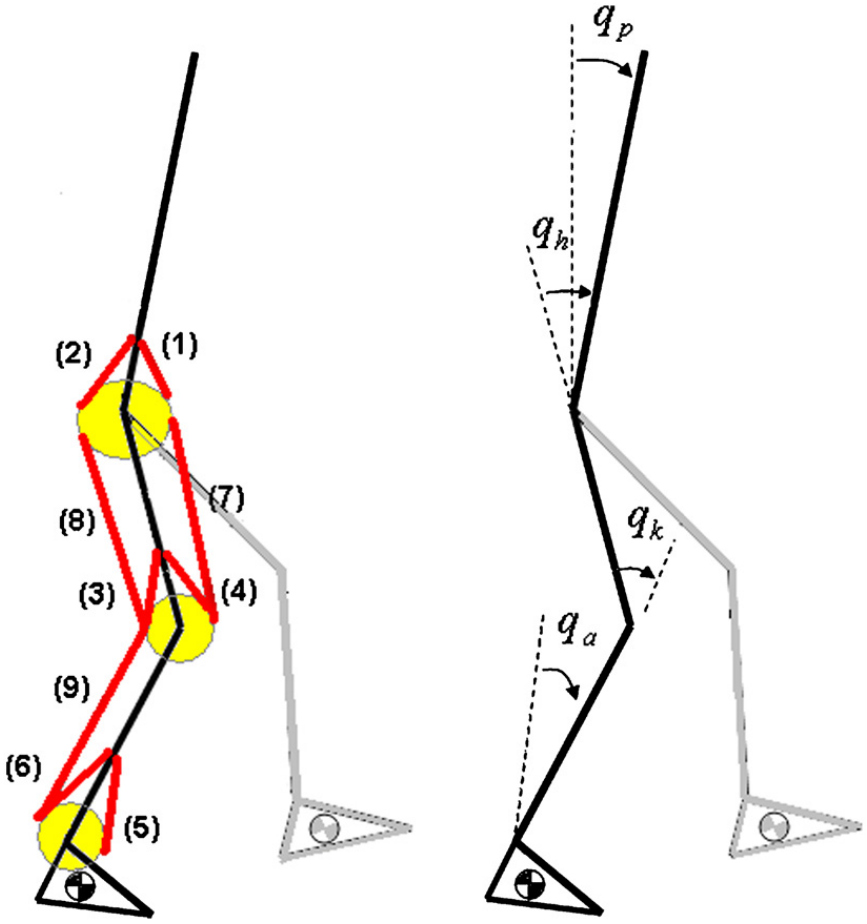

Fig. 1. (Left) Muscle model: (1) hip flexor (monoarticular muscle, e.g. Iliopsoas); (2) hip extensor (monoarticular muscle, e.g. Gluteus maximus); (3) knee flexor (monoarticular muscle, Biceps femoris short); (4) knee extensor (monoarticular muscle, e.g. Vastus); (5) ankle dorsiflexor (monoarticular muscle, e.g. Tibialis); (6) ankle plantarflexor (monoarticular muscle, e.g. Soleus); (7) hip–knee extensor (biarticular muscle, e.g. Rectus femoris); (8) hip–knee flexor (biarticular muscle, e.g. Biceps femoris long); (9) knee–ankle flexor (biarticular muscle, e.g. Gastrocnemius). (Right) Angle convention: q_a, q_k, and q_h represents ankle, knee, and hip angles, respectively for each leg, and q_p is the trunk pitch angle.

mates the relative position of ankle to hip in the swing leg. The estimated relative position is a criterion to decide the recovery strategy. When the estimated relative position is below a threshold (which indicates the early swing phase), muscular activations for the elevating strategy evoke. On the other hand, muscular activations provoke the lowering strategy when the estimated relative position is above the threshold (which indicates the late swing phase).

2.2. Model

In this section, neural-musculo-skeletal models are proposed to investigate the recovery behaviors of perturbed walking. Spinal stretch reflexes and voluntary control are appended to the previous model.

2.2.1. Musculo-skeletal model

Seven rigid segments in the sagittal plane represent a human body as in Fig. 1. A segment rotates at pivot joints with respect to an adjacent segment. High impedance around the knee joint represents the knee locking to hinder hyperextension. The overall body dynamics equation is in the form of

$$H(q)\ddot{q} + C(q, \dot{q}) - G(q) = \tau_M + \tau_E \quad (1)$$

where q is a vector of joint angles, τ_M represents a vector of joint torques generated by muscles and τ_E a vector of torques generated by ground interaction or any other influence. $H(q)$ is the inertia matrix and $C(q, \dot{q})$ is the centrifugal and Coriolis term, and $G(q)$ is the gravitational effect term. The body parameters summarized in Appendix A.

Muscular forces generate joint torques via muscle's moment arms

$$\tau_M = M^T F(l, \dot{l}, a) \quad (2)$$

where M is the moment arm matrix, l and $\dot{l}$ are vectors of muscle lengths and velocities, respectively, and a is a vector of muscular activation signals.

The muscular forces consist of active (F_a) and passive (F_p) ones, respectively modeled as follows:

$$F_p = [K_p(l_{eq} - l) - B_p\dot{l}]_+, \quad F_a = K_a(a)[l(a) - l]_+ - B_a(a)\dot{l},$$
$$F = [F_a + F_p]_+ \quad (3)$$

where l_{eq} is a vector of muscle lengths at an equilibrium position, K_p and B_p represents passive muscle stiffness and viscosity matrices, and $K_a(\cdot)$ and $B_a(\cdot)$ are active muscle stiffness and viscosity matrices as functions of the activation signal, and $[x]_+ = x$ if $x > 0$, and $[x]_+ = 0$ if $x \leq 0$.

The muscle force formulations substantially follow those employed by Katayama and Kawato (1993). The passive muscle stiffness and viscosity values are, respectively the elements of diagonal matrices K_p and B_p. The relative scales of the stiffness values are proportional to the cross-sectional area of the muscles (Brand et al., 1986). Then, using the intrinsic ankle joint stiffness known to be about 90 N m/rad (Fujita and Sato, 1998), the absolute values of the stiffness are determined. Viscosity values are set at a tenth of stiffness according to arm modeling study (Flash, 1987; Katayama and Kawato, 1993).

As in Jo and Massaquoi (2007), the active muscle stiffness and viscosity matrices are set in the form of

$$K_a(\mathrm{act}) = K_{a0}(\alpha[\mathrm{act}]_+ + \beta \min(\gamma[\mathrm{act}]_+, 1)),$$
$$B_a(\mathrm{act}) = B_{a0}(\alpha[\mathrm{act}]_+ + \beta \min(\gamma[\mathrm{act}]_+, 1)) \quad (4)$$

where K_{a0} and B_{a0} are constant 9×9 diagonal matrices, and α, β, γ are constants.

The constant K_{a0} and B_{a0} are, respectively set to be two and a half times of passive stiffness and viscosity based on the observation that stiffness and damping ratio (viscosity per the square root of stiffness) of human arm muscles increases up to 500% and 50%, respectively (Lacquaniti and Soechting, 1986).

Joint angular and muscle length coordinates are geometrically related

$$l = l_{eq} + M(q_{eq} - q), \quad \dot{l} = -M\dot{q} \quad (5)$$

where q_{eq} is the vector of joint angles at an equilibrium position. Therefore, joint angles and angular velocities from body dynamics are used to decide muscle lengths and length change required for the calculation of muscle force.

Then, to calculate muscle force completely according to the muscle model, the muscular activation signal is required. The alpha motor neuronal command via muscular activation dynamics provides the muscular activation signal below:

$$a = \mathrm{EC}(u_\alpha) \quad (6)$$

where $\mathrm{EC} = L^{-1}(\rho^2/(s+\rho)^2)$ $\rho = 30$ rad/s (Fuglevand and Winter, 1993), and s is the Laplace variable, L^{-1} is the inverse Laplace transform, and u_α is the alpha motor neuronal command.

2.2.2. Ground interaction

Contact between the foot and the ground is modeled at two points, the heel and the toe. (x^i, y^i) indicates the contact locations of heel and toe with i = heel, toe.

While the foot contacts the ground, the vertical reaction forces are modeled by

$$F^i_{gy} = -K_{gy}y^i - B_{gy}\dot{y}^i \quad (7)$$

where K_{gy} and B_{gy} are coefficients.

Horizontal reaction forces are modeled under slippery condition

$$F^i_{gx} = \begin{cases} K_{gx}(x^i_0 - x^i) - B_{gx}\dot{x}^i & |F^i_{gx}| \leq \mu_s |F^i_{gy}| \\ -\mu_k F^i_{gy}\,\mathrm{sign}(\dot{x}^i) & \text{otherwise} \end{cases} \quad (8)$$

where K_{gx} and B_{gx} are coefficients, μ_s the static frictional coefficient, μ_k the dynamic frictional coefficient, and x^i_0 is a position where contacts the ground initially.

The interaction between foot and ground is detected by tactile receptors on the foot. The signal from the receptor is expressed by R_t:

$$R_t = \begin{cases} 1 & \text{if } F^t_{gy} + F^h_{gy} > 0 \\ 0 & \text{if } F^t_{gy} + F^h_{gy} = 0 \end{cases} \quad (9)$$

For simplicity, detection is based on the total reaction force on the foot, which is a sum of reaction forces on the toe and heel. R_t is 1 when the foot contacts the ground and 0 otherwise. Therefore, the tactile receptors inform of whether each leg is at either swing or stance phase.

2.2.3. Feedforward spinal pattern generator

Experimental observations support a spinal locus for important rhythmic locomotor EMG pattern generation in humans (Dimitrijevic et al., 1998; Grasso et al., 2004; Calancie et al., 1994; Dietz and Harkema, 2004). An electrical stimulation to a local spot at spinal level led to generate alternate locomotion-like movement of the leg (Pinter and Dimitrijevic, 1999; Vogelstein et al., 2006). Interestingly, discrete pulse of electrical stimulation to a single spinal segment modulates multiple muscular activities. The phenomenon proposes the locomotive synergy network. A small number of simple pulses ($u_{PG,i}$) provide the whole muscular activation patterns ($u_{SP,j}$) periodically via the distributive synergy network. For the present model, the distributive network is simply expressed by a matrix W_S:

$$u_{SP} = W_S u_{PG} \quad (10)$$

Jo and Massaquoi (2007) proposed that rectangular pulses in a fixed sequence represent periodic neural stimuli. Each simple pulse is empirically chosen to be in the form of

$$u_{PG,i}(t) = s_{PG} \cdot 1[\cos(2\pi f_{PG} t - \phi_i) - h_i]_+, \quad i = 1, 2, 3, 4 \quad (11)$$

where $1[x]_+ = 1$ if $x > 0$ and $1[x]_+ = 0$ otherwise, and S_{PG}, f_{PG}, ϕ_i, h_i are constant parameters.

Fig. 2 illustrates the spinal pattern generation combined with the locomotive synergy network. Fig. 2(top) illustrates the feedforward pulses and Fig. 2(bottom) shows the activation patterns from the spinal pattern generator via the distributive network. The whole mechanism is probably located at spinal cord level (Pinter and Dimitrijevic, 1999). For computational simplicity, the feedforward pulses activate monoarticular muscles only in the model (Jo and Massaquoi, 2007).

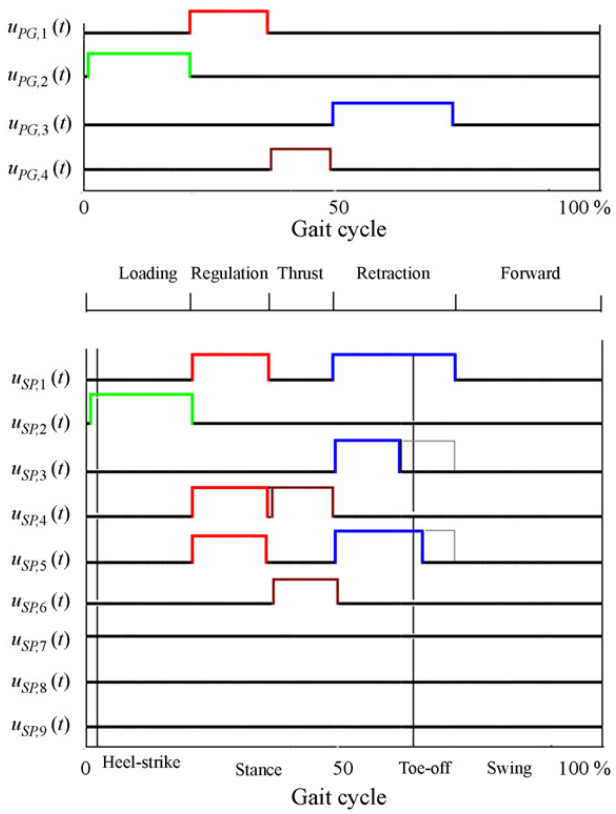

Fig. 2. Spinal binary activation pulses (top) and pulse patterns from spinal pattern generator to muscles (bottom) for simulation. Firing intensity is modeled by a rectangular pulse for simplicity.

2.2.4. *Reflexes*

2.2.4.1. Vestibulo-spinal reflex model. It is assumed that the vestibular system concerns maintaining the upper body vertical. The pitch angle of the upper body is represented as q_p and therefore the reference of its vertical position is set to be $q_{P,ref} = 0$ (Fig. 3). q_p is detected by the vestibular system. In the case of non-horizontal surfaces, the trunk-head segment pitch estimate is presumably adjusted on the basis of or replaced by further visual and/or vestibular input. However, this issue is not examined here.

The vestibulo-spinal reflex is simply modeled as

$$u_v = [W_v(k_v(q_{P,ref} - q_p) - b_v\dot{q}_p)]_+ \quad (12)$$

where W_v is a distribution vector, and k_v and b_v are, respectively proportional and derivative gains.

2.2.4.2. Spinal segmental reflex model. For generation of normal walking motions, the model includes a feedback reflex, whose mechanism is the presynaptic inhibition (Baxendale and Ferrell, 1981; Brooke et al., 1997; Duysens et al., 2000; Rudomin and Schmidt, 1999). The reflex sometimes truncates the feedforward pulses for stable gait implementation. The suppression is shown by dotted lines in Fig. 2:

$$u_{rx} = -W \cdot 1[\hat{q} - q_0]_+ \quad (13)$$

where each element of $q_0 = [\,q_{a,0} \quad q_{k,0} \quad q_{h,0}\,]^T$ represents a threshold value, and $\hat{q} = [\,q_a(t - T_{pr,a}) \quad q_k(t - T_{pr,k}) \quad q_h(t - T_{pr,h})\,]^T$ is the sensed joint information delayed from the each joint to the spinal cord.

The above equation represents an inhibition that suppresses the activity of the feedforward pattern generator when sensed information indicates each joint position passing over a critical value so that the joint does not rotate excessively further.

In the feedforward pattern generation, the pulse in $u_{SP,6}$ during "Thrust" epoch provides muscular activation to the ankle plantarflexor (soleus) for forward push at toe-off. A phase-dependent reflex feedback control helps to adjust the activation intensity depending on the walking posture. If the COM with respect to a stance leg at push-off is smaller than a normal

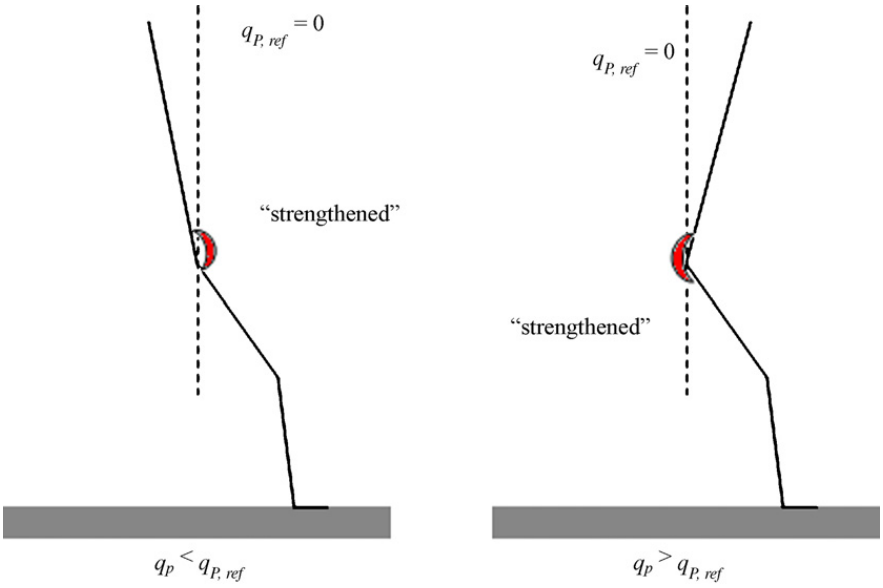

Fig. 3. Vestibulo-spinal reflex feedback model.

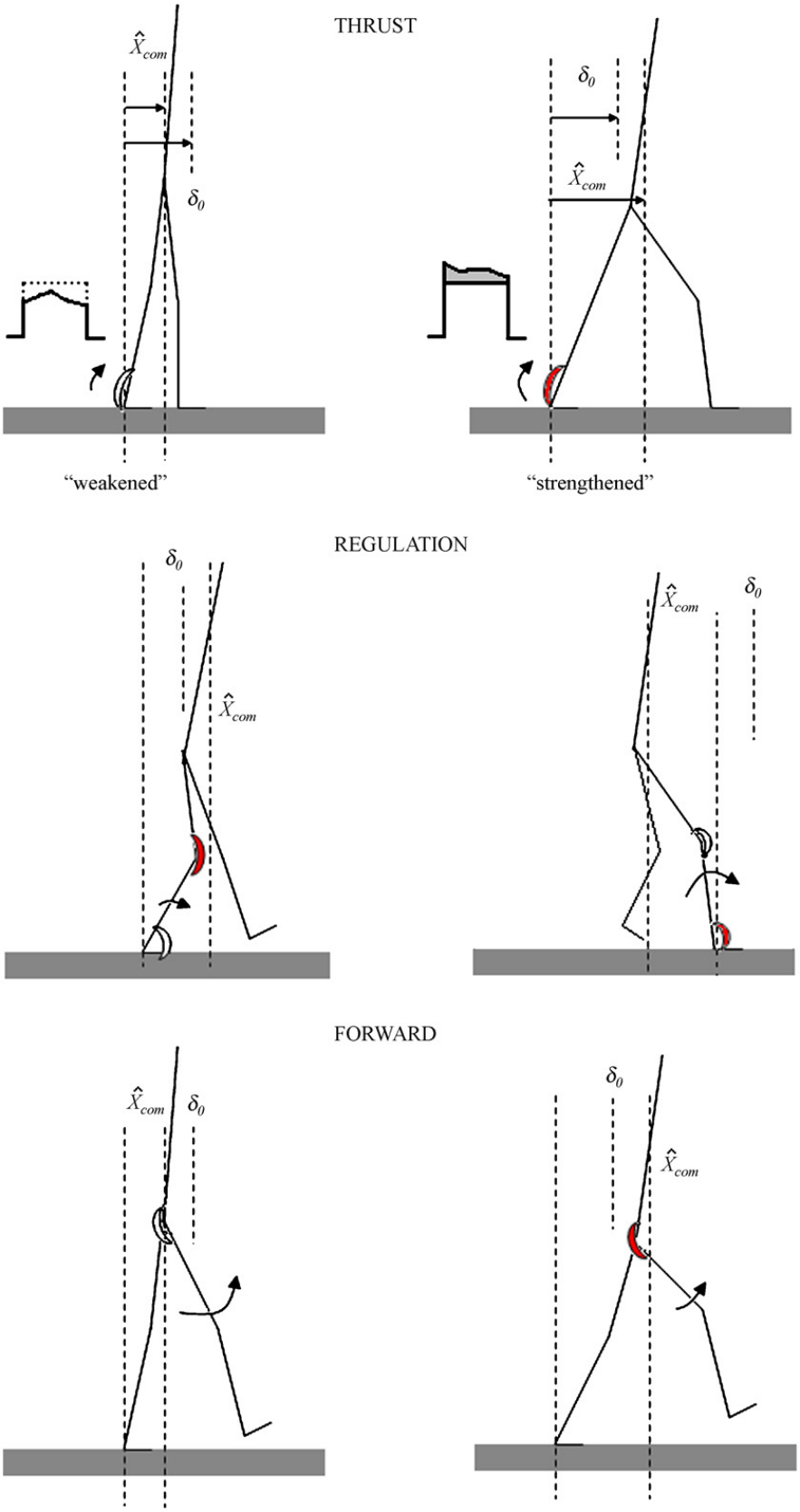

Fig. 4. Reflex models, the filled crescent represents augmentation of muscular activation, and the empty crescent attenuation of muscular activation by the reflexes.

value, i.e., the step size is small, the pulse gets weaker to protect the upper body from excessively rotating forward. On the other hand, if the COM is greater, i.e., the step size is large, the pulse gets augmented to earn sufficient forward thrust (Fig. 4). A simple feedback reflex of the mechanism is proposed as

$$\Delta u = k_t(\hat{x}_{\mathrm{com}}(t - T_{\mathrm{sp}}) - \delta_0) \text{ during "Thrust" epoch}$$

$$\text{and} \quad \tilde{u}_{\mathrm{SP},6} = u_{\mathrm{SP},6} + \Delta u$$

where T_{sp} is the transmission neural delay from the supraspinal to the spinal system, and $\hat{x}_{\mathrm{com}}$ is the estimated COM from Eq. (18).

Responding to perturbation, either augmented or weakened forward thrust is applied to the body as above. During "Regulation" epoch, which is roughly consistent with the mid-stance phase, the ankle dorsiflexor in a stance leg prefers to be quickly further activated to move the COM forward away from the pivot point or less activated to drag the withdrawal of the COM (Fig. 4). Either knee flexor attenuation or augmentation also helps

$$\Delta u = k_{\mathrm{r}}(\hat{x}_{\mathrm{com}}(t - T_{\mathrm{sp}}) - \delta_0) \text{ during "Regulation" epoch}$$

$$\text{and} \quad \tilde{u}_{\mathrm{SP},3} = u_{\mathrm{SP},3} + \Delta u, \qquad \tilde{u}_{\mathrm{SP},5} = u_{\mathrm{SP},5} - \Delta u$$

Then, the swing leg also has to be controlled by phase-dependent reflex. When forward thrust is weakened, the hip extensor is less activated during the swing phase ("Forward" epoch) to attain a sufficient step size by allowing the hip flexor to evoke a larger step. On the other hand, when forward thrust is large, the hip extensor needs to be further activated during the swing phase to hold the action of the hip flexor because the swing leg already obtained sufficient inertia force for excessive swing motion by push-off. If the hip extensor remained unchanged, the step size would be greater than normal.

$$\Delta u = k_{\mathrm{f}}(\hat{x}_{\mathrm{com}}(t - T_{\mathrm{sp}}) - \delta_0) \text{ during "Forward" epoch}$$

$$\text{and} \quad \tilde{u}_{\mathrm{SP},2} = u_{\mathrm{SP},2} + \Delta u$$

In summary, feedback reflexes affect the feedforward pulse waveforms from the pattern generator:

$$u_{sx} = \tilde{u}_{\mathrm{SP}} + u_{\mathrm{r}x} + u_{\mathrm{v}} \tag{14}$$

where the resultant neural signal is notated as u_{sx}.

2.2.5. Supraspinal long-loop feedback control

Fig. 5 shows the cerebrocerebellar system to represent the supraspinal long-loop feedback control. The cerebrocerebellar control was adapted from previous studies (Jo and Massaquoi, 2004, 2007; Takahashi, 2006). The cerebellar control is hypothetically modeled based on the neuroanatomy in the cerebellar cortex (Jo and Massaquoi, 2004). In Fig. 5(top), x_{cb} is the input to the cerebellar cortex through the mossy fibers, u_{cb} is the output from the deep cerebellar nuclei. Adaptive process is beyond the present study. Therefore, the input through the climbing fibers is not considered because the signal is known to be related to adaptation (Ito, 1997). The cerebellar input signal $x_{\mathrm{cb}}(t)$ directly excites the deep cerebellar nuclei and the Purkinje cell through the ascending segment. Then, the Purkinje cell inhibits the deep cerebellar nuclei. Therefore, there are two neural pathways between the input and output (Fig. 5(top)). Considering the tiny neural transmission delay between the two neural pathways, a linear signal processing model is described by

$$w_1 x_{\mathrm{cb}}(t) - w_2 x_{\mathrm{cb}}(t - \Delta t) \approx w_1 \dot{x}_{\mathrm{cb}}(t) + (w_1 - w_2) x_{\mathrm{cb}}(t - \Delta t)$$

where Δt is neural transmission delay and w_1, w_2 are coefficients representing the intensity of activity.

Therefore, the cerebellar control is set to be

$$u_{\mathrm{cb}} = g_{\mathrm{b}} \dot{x}_{\mathrm{cb}} + g_{\mathrm{k}} x_{\mathrm{cb}} \tag{15}$$

where g_{k} and g_{b} are, respectively, proportional and derivative control gains. The g_{b} is used to scale differential (high frequency) signals attributed to lateral cerebellum whose output is through the dentate nuclei (Massaquoi, 1999). While it has been noted that there is apparently a complete somatotopic body representation within the dentate (Thach et al., 1992), the dentate is generally seen to be less active with truncal and leg movement rather than with arm and hand movements. This is also in comparison with the activities of the interpositus and fastigial nuclei that are strongly involved in leg movement control (Amstrong and Edgley, 1988; Mori et al., 2004) and presumably represented as g_{k} in the model.

The recurrent integration loop (with gain i_{r}) between the cerebellar and cerebral systems is consistent with a reverberating circuit involving precerebellar brainstem nuclei and the signal on the projection pathway may be comparable with efference-copy discharge (Allen and Tsukahara, 1974; Massaquoi and Topka, 2002). Functionally, the recurrent loop provides the phase lead useful for delay compensation. The sensorimotor cortical role is modeled by an integrator (with gain i_{c}) corresponding to a computational study (Karameh and Massaquoi, 2005), and the afferent signal pathway bypassing the sensorimotor cortices is represented by gain f.

In the proposed model, each leg is supervised by two cerebrocerebellar channels of the long-loop feedback, i.e., stance and swing control channels.

The cerebellar input $x_{\mathrm{cb},i}$ to each cerebellar control is computed as follows:

$$x_{\mathrm{cb},i} = L^{-1}\{(s + i_{\mathrm{r}})^{-1}(i_{\mathrm{c}}(u_{\mathrm{ref},i} - p_i^{\mathrm{T}}\hat{q}_i(s)) - sfp_i^{\mathrm{T}}\hat{q}_i(s))\} \tag{16}$$

where $u_{\mathrm{ref},i}$ is the reference set point, and $p_i^{\mathrm{T}}\hat{q}_i$ represents the ascending information to the cerebrocerebellar channel: p_i, and $\hat{q}_i$ are clarified in the next section ($i = 1, 2$).

2.2.5.1. Stance leg control. For a cerebrocerebellar channel of stance leg control, $u_{\mathrm{ref},1}$ is set to 25 cm. This indicates a desired goal of gait is to locate the body's COM in front of the stance leg during the stance phase. The COM position relative to the stance foot is linearly approximated as

$$\hat{x}_{\mathrm{com}} = \frac{m_1}{m_1 + m_2 + m_3} r_1 \sin q_{\mathrm{a}}(t - T_{\mathrm{spr,a}}) + \frac{m_2}{m_1 + m_2 + m_3} \times (l_1 \sin q_{\mathrm{a}}(t - T_{\mathrm{spr,a}}) + r_2 \sin(q_{\mathrm{a}}(t - T_{\mathrm{spr,a}})$$

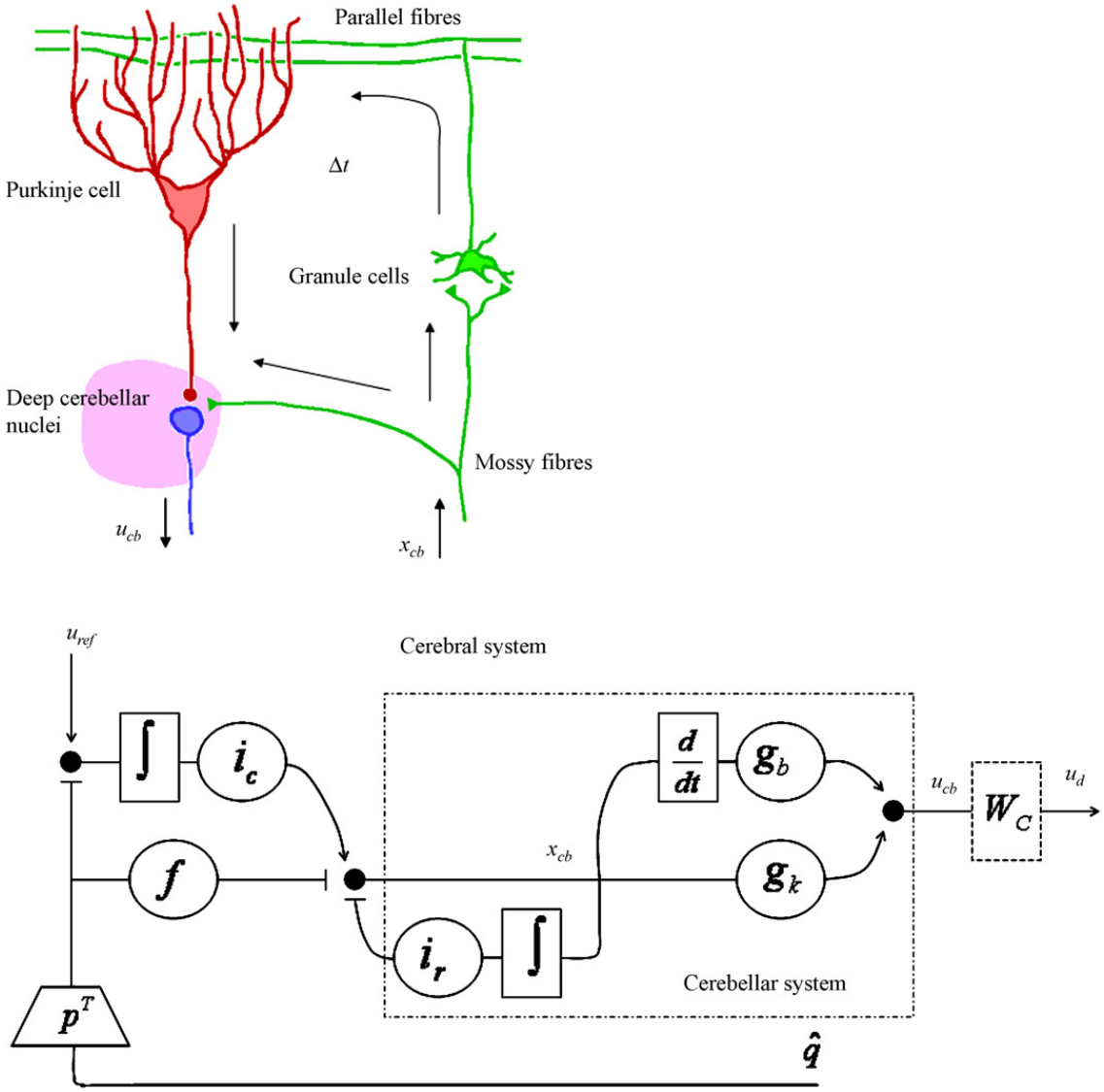

Fig. 5. Supraspinal long-loop feedback control model: (top) cerebellar cortex model; (bottom) cerebrocerebllar system model. Bars indicate inhibitions, and arrows excitations.

$$
\begin{aligned}
&+q_{\mathrm{k}}(t-T_{\mathrm{aff,k}}))) + \frac{m_3}{m_1+m_2+m_3}(l_1 \sin q_{\mathrm{a}}(t-T_{\mathrm{spr,a}}) \\
&+l_2 \sin(q_{\mathrm{a}}(t-T_{\mathrm{spr,a}}) + q_{\mathrm{k}}(t-T_{\mathrm{spr,k}})) \\
&+r_3 \sin(q_{\mathrm{a}}(t-T_{\mathrm{spr,a}}) + q_{\mathrm{k}}(t-T_{\mathrm{spr,k}}) + q_{\mathrm{h}}(t-T_{\mathrm{spr,h}}))) \\
\approx\ & \frac{m_1 r_1 + m_2(l_1+r_2) + m_3(l_1+l_2+r_3)}{m_1+m_2+m_3} q_{\mathrm{a}}(t-T_{\mathrm{spr,a}}) \\
&+\frac{m_2 r_2 + m_3 l_2}{m_1+m_2+m_3} q_{\mathrm{k}}(t-T_{\mathrm{spr,k}}) + \frac{m_3 r_3}{m_1+m_2+m_3} \\
&\times q_{\mathrm{h}}(t-T_{\mathrm{spr,h}}) \qquad (17)
\end{aligned}
$$

where q_{a}, q_{k}, and q_{h} are ankle, knee, and hip joint angles of stance leg; m_i, r_i, and l_i are, respectively mass, length between COM and lower end, and length of each body segment ($i=1$: lower leg, $i=2$: upper leg, $i=3$: trunk-head segment).

$T_{\mathrm{spr}} = [T_{\mathrm{spr,a}} \quad T_{\mathrm{spr,k}} \quad T_{\mathrm{spr,h}}]^{\mathrm{T}}$ are the afferent signal transmission delays including spinal and peripheral components from limb joint to head.

Therefore,

$$
\begin{aligned}
\hat{x}_{\mathrm{com}} &= p_{11} q_{\mathrm{a}}(t-T_{\mathrm{spr,a}}) + p_{12} q_{\mathrm{k}}(t-T_{\mathrm{spr,k}}) + p_{13} q_{\mathrm{h}}(t-T_{\mathrm{spr,h}}) \\
&= p_1^{\mathrm{T}} \hat{q}_1 \qquad (18)
\end{aligned}
$$

where $p_1 = [\, p_{11} \quad p_{12} \quad p_{13} \,]^{\mathrm{T}}$ are constants, and the scaling factors p_{1i} were consistent with coefficients in Eq. (17), and $\hat{q}_1 = [\, q_{\mathrm{a}}(t-T_{\mathrm{spr,a}}) \quad q_{\mathrm{k}}(t-T_{\mathrm{spr,k}}) \quad q_{\mathrm{h}}(t-T_{\mathrm{spr,h}}) \,]^{\mathrm{T}}$.

The signal from tactile receptor on foot to sense ground contact is assumed to determine which leg is in stance or in swing. This cerebrocerebellar channel activates only while the leg touches the ground. The ground contact is indicated by $R_{\mathrm{t}}(t-T_{\mathrm{spr,a}}) = 1$ from Eq. (9).

2.2.5.2. Swing leg control. For a cerebrocerebellar channel of a swing leg control, $u_{\mathrm{ref},2}$ is set to be 25 cm. This indicates that a desired goal of gait is to locate the ankle (or foot) position in front of the hip position during the swing phase. The relative distance between the ankle and the hip positions is linearly approximated as

$$\hat{x}_{\mathrm{ah}} = l_3 \sin(q_{\mathrm{h}}(t-T_{\mathrm{spr,h}})-q_{\mathrm{p}}(t))+l_2 \sin(q_{\mathrm{h}}(t-T_{\mathrm{spr,h}}) - q_{\mathrm{p}}(t) + q_{\mathrm{k}}(t-T_{\mathrm{spr,k}})) \approx l_2 q_{\mathrm{k}}(t-T_{\mathrm{spr,k}}) + (l_2+l_3) q_{\mathrm{h}}(t-T_{\mathrm{spr,h}}) - (l_2+l_3) q_{\mathrm{p}}(t) \quad (19)$$

where q_{k}, q_{h}, and q_{p} are, respectively knee, and hip joint angles of swing leg, and trunk pitch angle.

Therefore,

$$\hat{x}_{\mathrm{ah}} = p_{21} q_{\mathrm{k}}(t-T_{\mathrm{spr,k}}) + p_{22} q_{\mathrm{h}}(t-T_{\mathrm{spr,h}}) + p_{23} q_{\mathrm{p}}(t) = p_2^{\mathrm{T}} \hat{q}_2 \quad (20)$$

where $\hat{q}_2 = [\, q_{\mathrm{k}}(t-T_{\mathrm{spr,k}}) \quad q_{\mathrm{h}}(t-T_{\mathrm{spr,h}}) \quad q_{\mathrm{p}}(t-T_{\mathrm{spr,h}})]^{\mathrm{T}}$.

Each cerebrocerebellar channel is turned on and off by the tactile detection of the ground.

In both swing and stance leg controls, the descending signal is expressed as

$$u_{\mathrm{c},i} = W_{\mathrm{C},i} u_{\mathrm{cb},i} \quad (21)$$

where $W_{\mathrm{C},i}$ is presumably a distribution matrix in either cerebral cortical area 4 and i indicates either swing or stance phase ($i = 1$: stance, $i = 2$: swing).

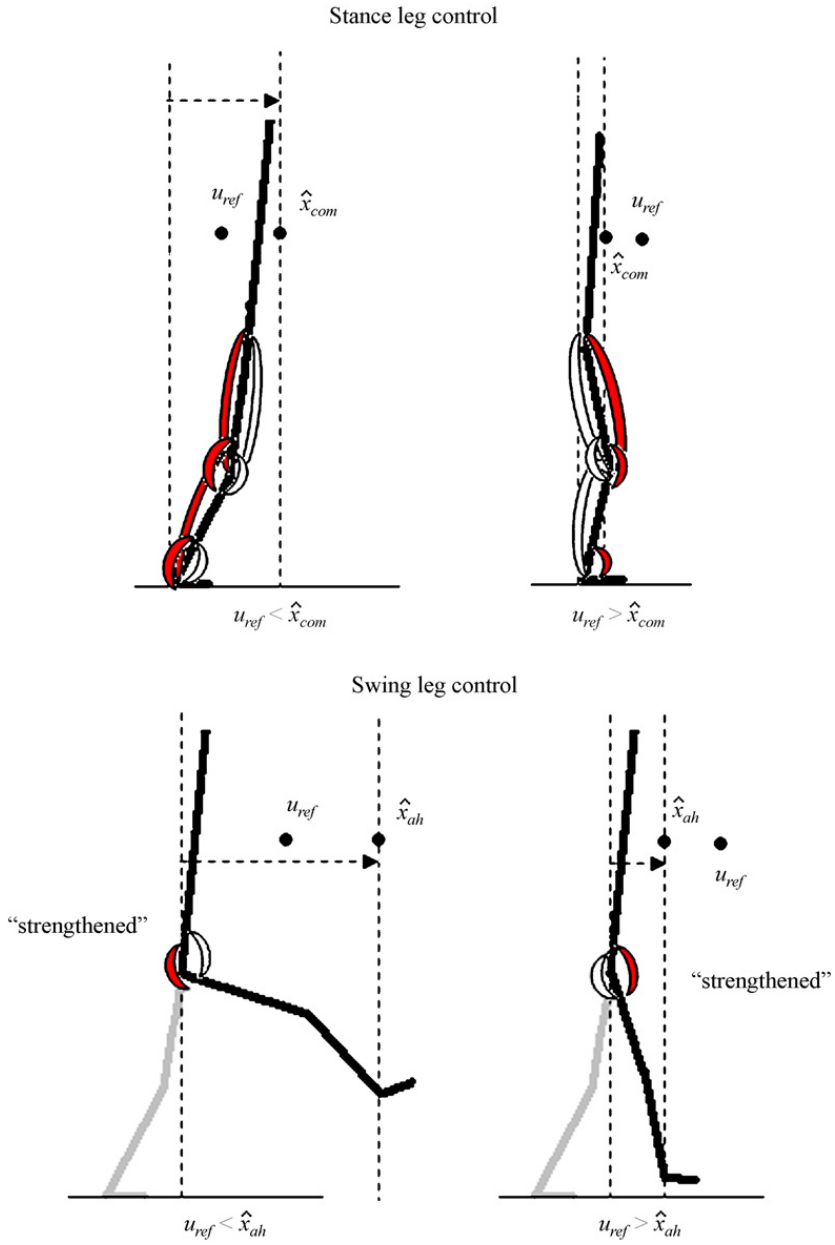

Fig. 6. The supraspinal (cerebrocerebellar) control over the stance and swing legs. Filled crescents indicate that muscular activation is strengthened, and empty crescents indicate that muscular activation is weakened.

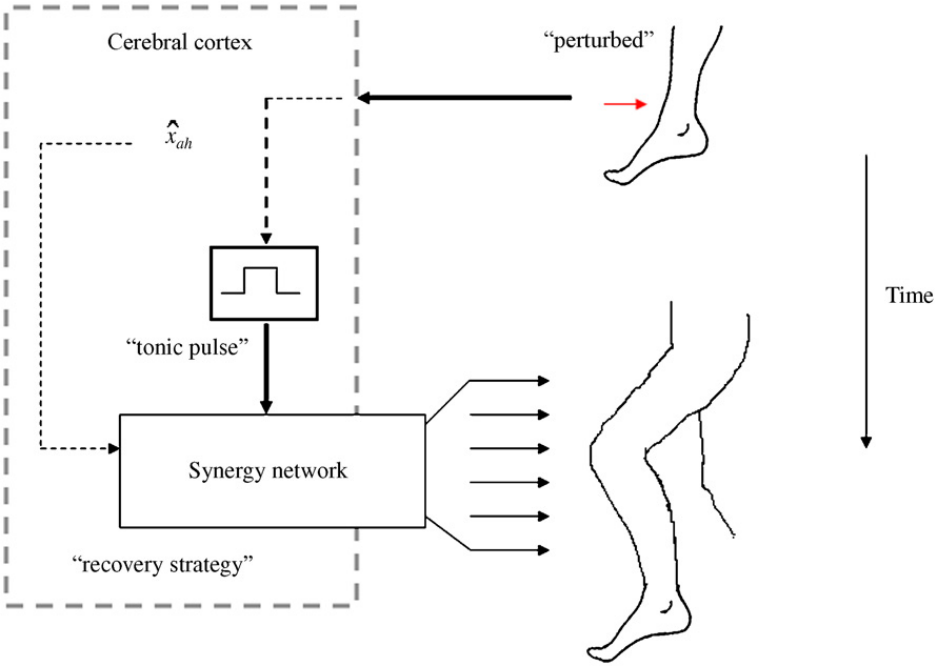

Fig. 7. A model of the long-loop reflex through the cortex.

This cerebrocerebellar channel activates only while the leg is in swing phase. The swing phase is indicated by $R_t(t - T_{spr,a}) = 0$ from Eq. (9) (Fig. 6).

2.2.6. Long-loop reflex through the cortex

Let $R_c(t)$ be the signal of the cutaneous receptor that detects the perturbation (Fig. 7).

$R_c(t) = 1$ when the perturbation is detected and $R_c(t) = 0$ otherwise:

$$u_l = 1 \cdot R_c(t - T_{spr}) \tag{22}$$

where u_l represents the descending pulse signal to elicit the long-loop response. The sensory signal ascends to the cerebral cortex via neural transmission delays.

The descending signal u_l is conveyed to the alpha motor neurons through the distribution (synergy) network W_l. The distribution network distributes the descending pulse to activate specific muscles around both legs so as to execute an appropriate recovery behavior. The distribution network would be consistent with the neural networks between the cortex and the spinal cord. A specific location does not matter for current study.

Depending on the swing leg position, different distribution networks operate. It is assumed that the swing leg position is informed by $\hat{x}_{ah}$ in Eq. (20).

Therefore,

$$W_l(\hat{x}_{ah}) = \begin{cases} W_{l,ES} & \text{if } \hat{x}_{ah} < x_T \\ W_{l,LS} & \text{if } \hat{x}_{ah} \geq x_T \end{cases} \tag{23}$$

where $W_{l,ES}$ is the synergy network for elevating strategy implementation, $W_{l,LS}$ for lowering strategy implementation and x_T is a threshold value (Fig. 8).

The descending pathway also contains neural delays. Therefore,

$$u_d = W_l(\hat{x}_{ah}) u_l(t - T_{spr}) \tag{24}$$

The alpha motor neuronal command is obtained by the sum of the overall neural commands.

$$u_\alpha = \sum_i u_{c,i} + \tilde{u}_{SP} + u_d \tag{25}$$

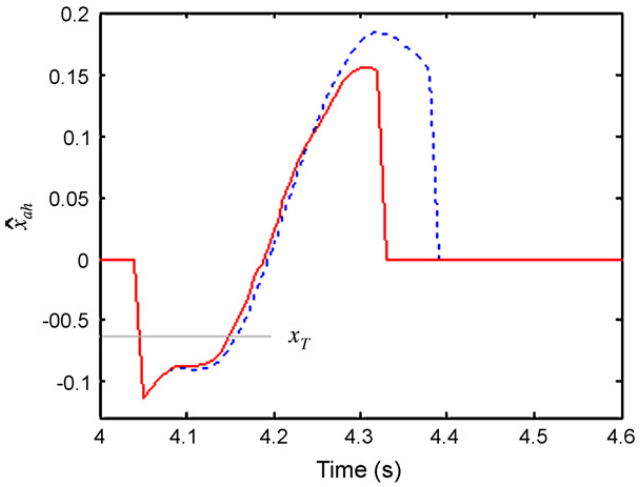

Fig. 8. Simulated trajectory of estimated swing position (!$\hat{x}_{ah}$): the dotted line shows elevating strategic motion and the solid line lowering strategic motion, the elevating strategy will be evoked if the perturbation is detected while $\hat{x}_{ah}$ is below x_T and the lowering strategy vice versa, $\hat{x}_{ah}$ is estimated in the cerebral cortex only in the swing phases.

2.3. Simulations

For simulation, closed-loop transmission delays are taken to be 60, 70 and 80 ms for long-loop responses to and from the hip, knee, and ankle, respectively. This is based on 50 m/s neural conduction velocity and five synaptic delays of less than 1 ms. For the spinal reflex-loops, 30, 35 and 40 ms are assigned, respectively to and from the hip, knee, and ankle. The muscular activation dynamics (Eq. (6)) also has effect on lagging signals.

While the model generates steady walking, a lower leg is perturbed backward during either the early or the late swing phase. This simulation test is similar to the experiment performed in Cordero et al. (2003, 2004). This simulation test is to realize typical human recovery strategies depending on swing phase by the proposed neuro-musculo-skeletal walking model. An impulsive force is backwardly applied to the COM of a swinging leg. The rectangular force is determined with the magnitude and the duration. The duration is fixed to be 150 ms based on the observation that the swing phase has generally the duration of about 300 ms for normal walking simulations. Early swing perturbation is applied just after swing phase begins and late swing perturbation is applied after mid-swing phase. Different values of force magnitude F_p are tested.

The body dynamics is executed using the SimMechanics 2.4, and the other system models are constructed using Simulink 6.4 in the Matlab R2006a (Mathworks Inc., Natick, MA, USA). The forward dynamic simulation is performed with the embedded ode45 integrator.

3. Results

3.1. Preliminary result

With no perturbation, normal walking motion at the regular speed of 1.25 m/s is realized (Fig. 9).

Looking at each joint motion, the ankle joint is always perturbed due to interaction with the ground. However, knee and hip joint motions draw limit cycles. Therefore, the model absorbs the interaction effect at level of ankle joint.

The sensitivity analysis of the model to changes in model parameters is considered. Each model parameter associated with the supraspinal and spinal systems is either 30% decreased or increased. Walking motion is simulated with the change and compared to normal walking simulation with no change in a nominal set of model parameters (the parameter values are summarized in Appendix A). Fig. 10 illustrates walking motions in the joint space with each parameter change. It is observed that the model can generally simulate stable walking even when a model parameter is changed. Stable walking can be achieved with f up to 25% increase from its nominal value. A decrease of both k_r and k_f implements unrest walking motion, but does not result in loss of stability. Either increase or decrease of g_k causes a slower

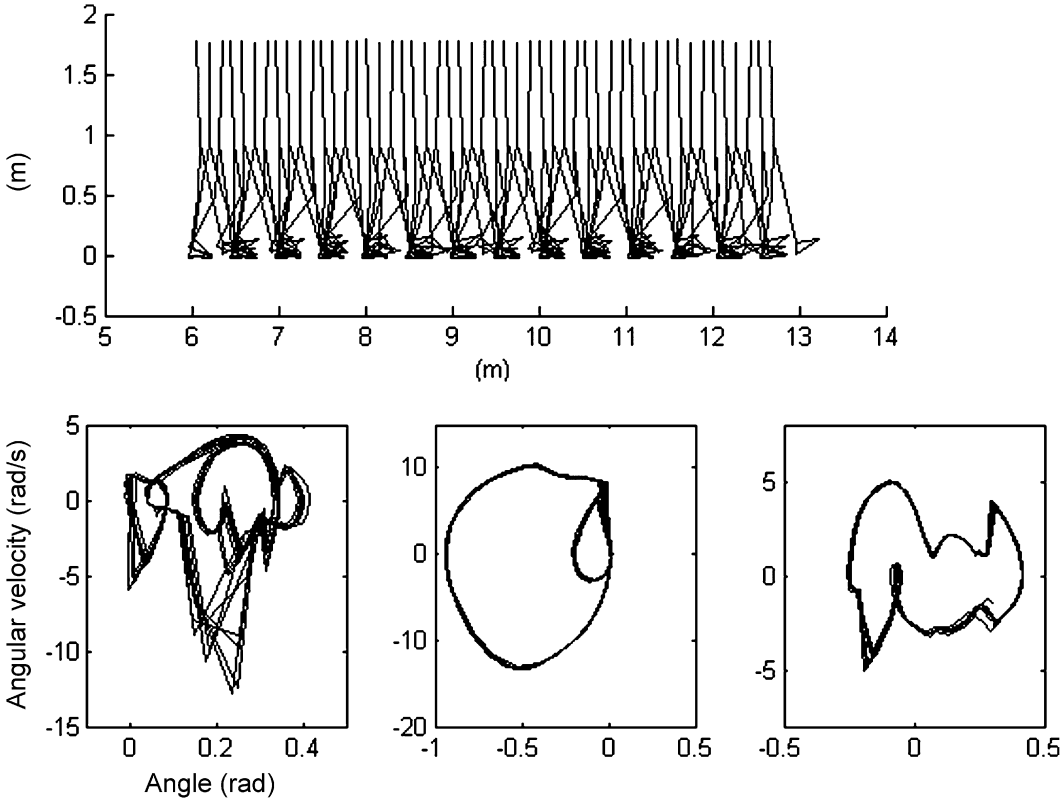

Fig. 9. The simulated normal walking.

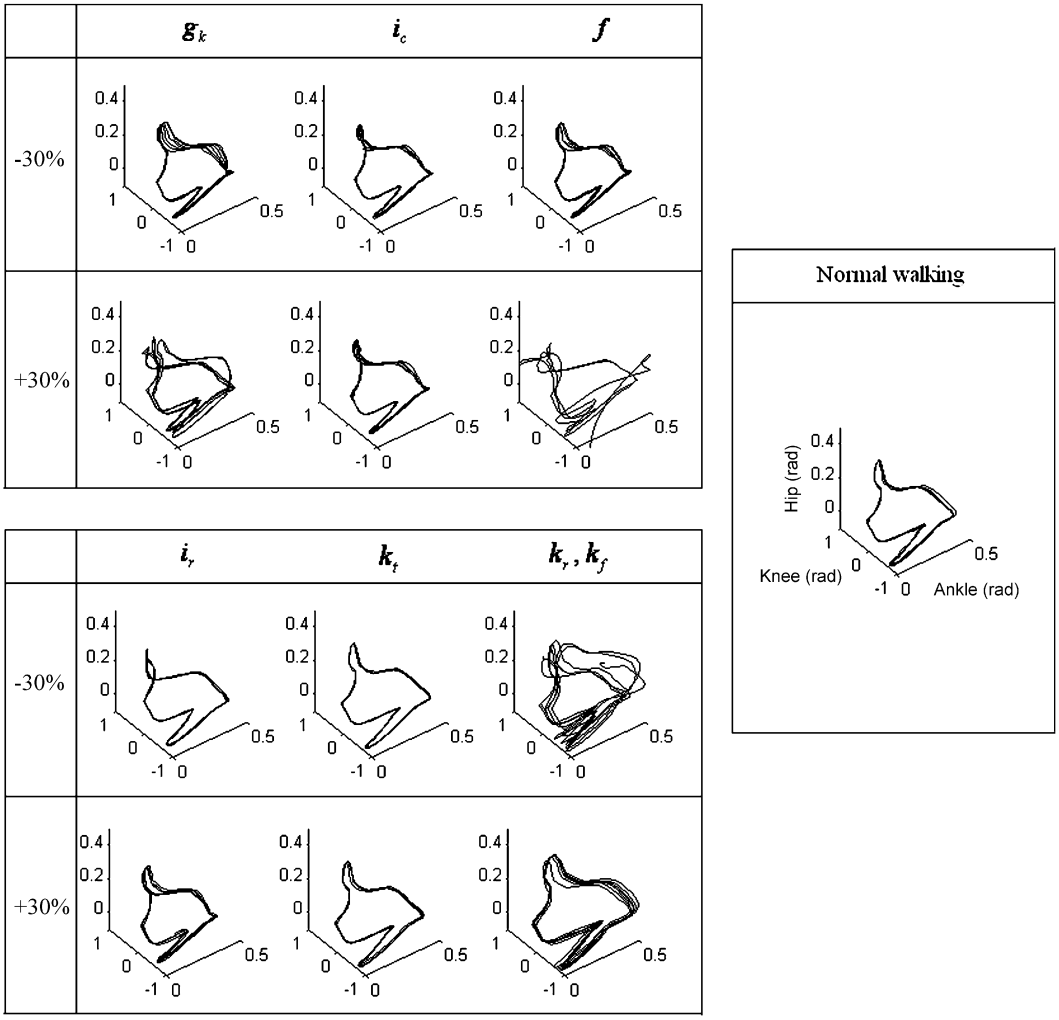

Fig. 10. Sensitivity to neural parameters; simulated motions with each parameter increased by 30% and decreased by 30% are drawn and compared with nominal walking motion with no change of parameters.

convergence to steady walking motion, but does not lose stability. The walking motion is less sensitive to i_c, i_r and k_t.

3.2. Recovery simulation from perturbed walking

A 70 N force is applied to the COM of a swinging leg ($F_p = 70$) in either the early or late swing phase. The perturbed leg for simulation is the right leg. The simulated responses are shown, respectively in Figs. 11 and 12.

Fig. 11 shows, in comparison with normal walking, each angular flexion increases during the recovery behavior against the early swing perturbation. In Fig. 12, ankle excursion increases while the other joints rotate less during the recovery behavior against the late swing perturbation.

To investigate the effectiveness of the proposed neural mechanism, long-loop reflex through the cortex for recovery strategies, the simulation is implemented with no long-loop reflex under the same condition of either early or late swing perturbations. Then, it is demonstrated that the model fails to recover against early swing perturbation in Fig. 13a. The model with no long-loop reflex in case of the late swing perturbation can maintain walking against up to an amount of perturbation intensity ($F_p = 90$). However, as the perturbation intensity increases, the model cannot recover stable walking posture without the long-loop reflex (Fig. 13b). Therefore, the simulated study proposes that lowering strategy promoted by the long-loop reflex help provide more robust recovery behavior.

Fig. 14 shows the time intervals of the swing phase from simulations. In normal walking, the time interval is 0.32–0.33 s over gaits. In the early swing perturbation, the time interval remains relatively consistent. In the late swing perturbation, the time interval of the perturbed swinging leg (right leg) is shorter just after the perturbation and returns to the normal interval.

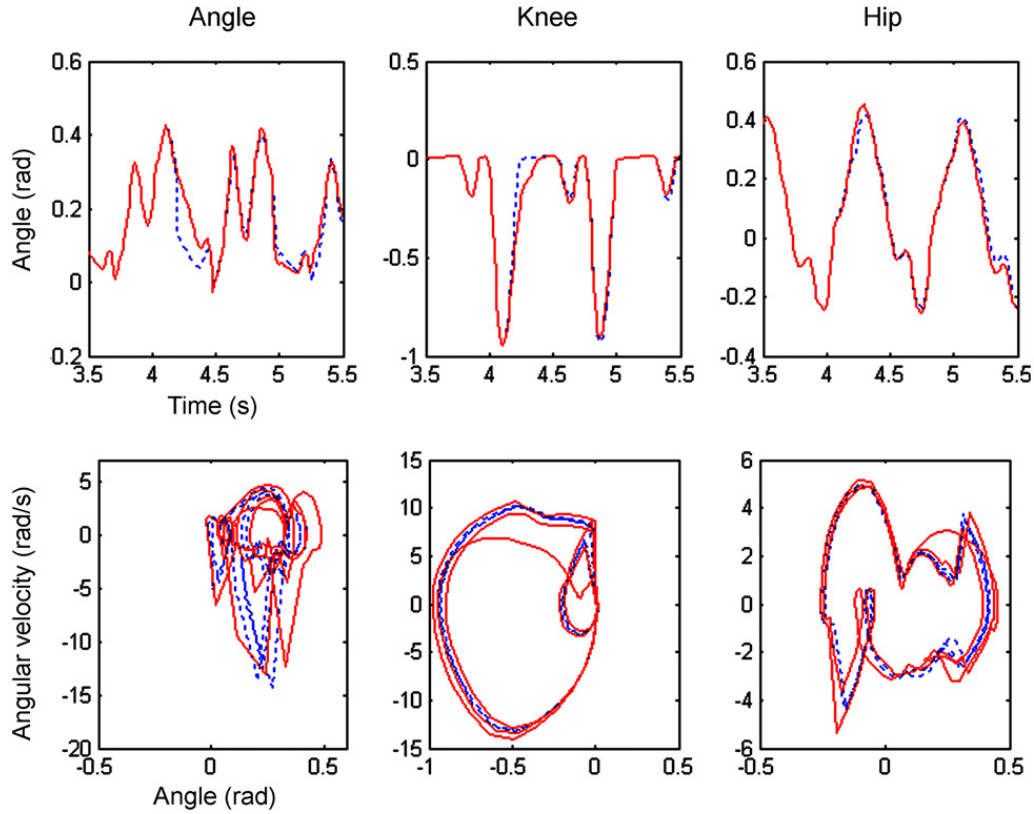

Fig. 11. Simulated recovery responses from perturbation in the early swing phase: (top) ankle, knee, and hip joint trajectories; (bottom) phase plots (dotted: normal walking, solid: perturbed walking).

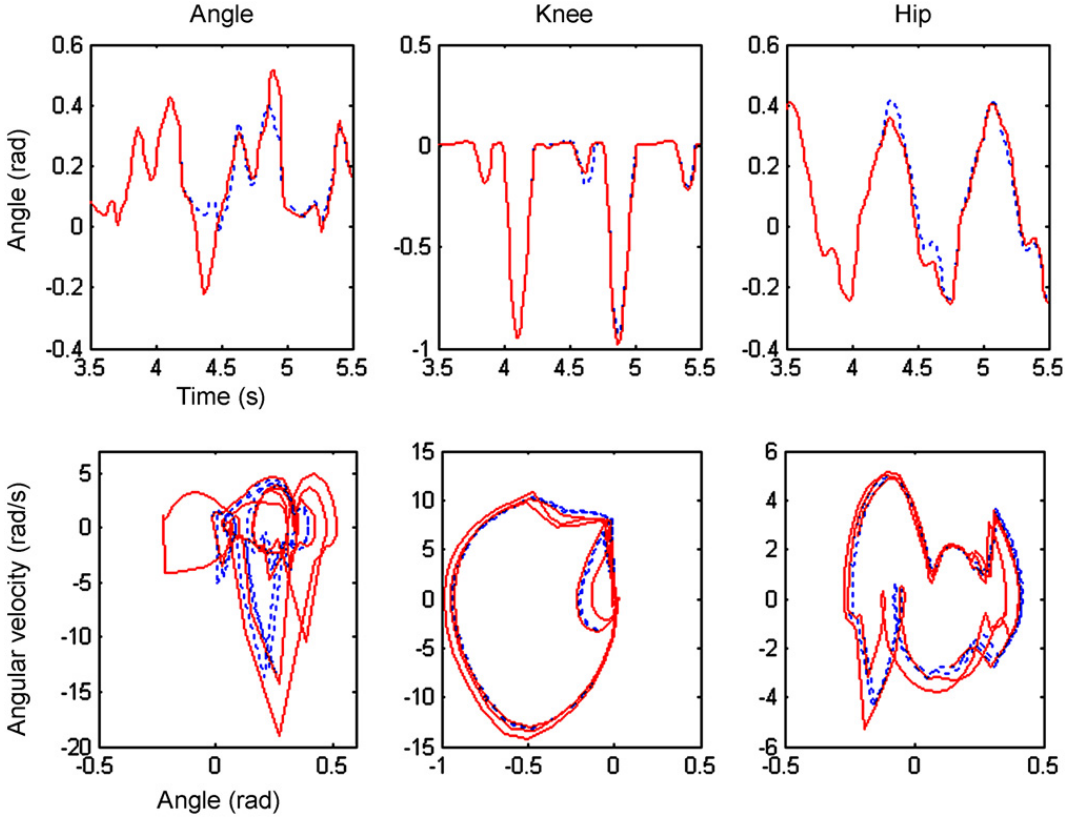

Fig. 12. Simulated recovery responses from perturbation in the late swing phase: (top) ankle, knee, and hip joint trajectories; (bottom) phase plots (dotted: normal walking, solid: perturbed walking).

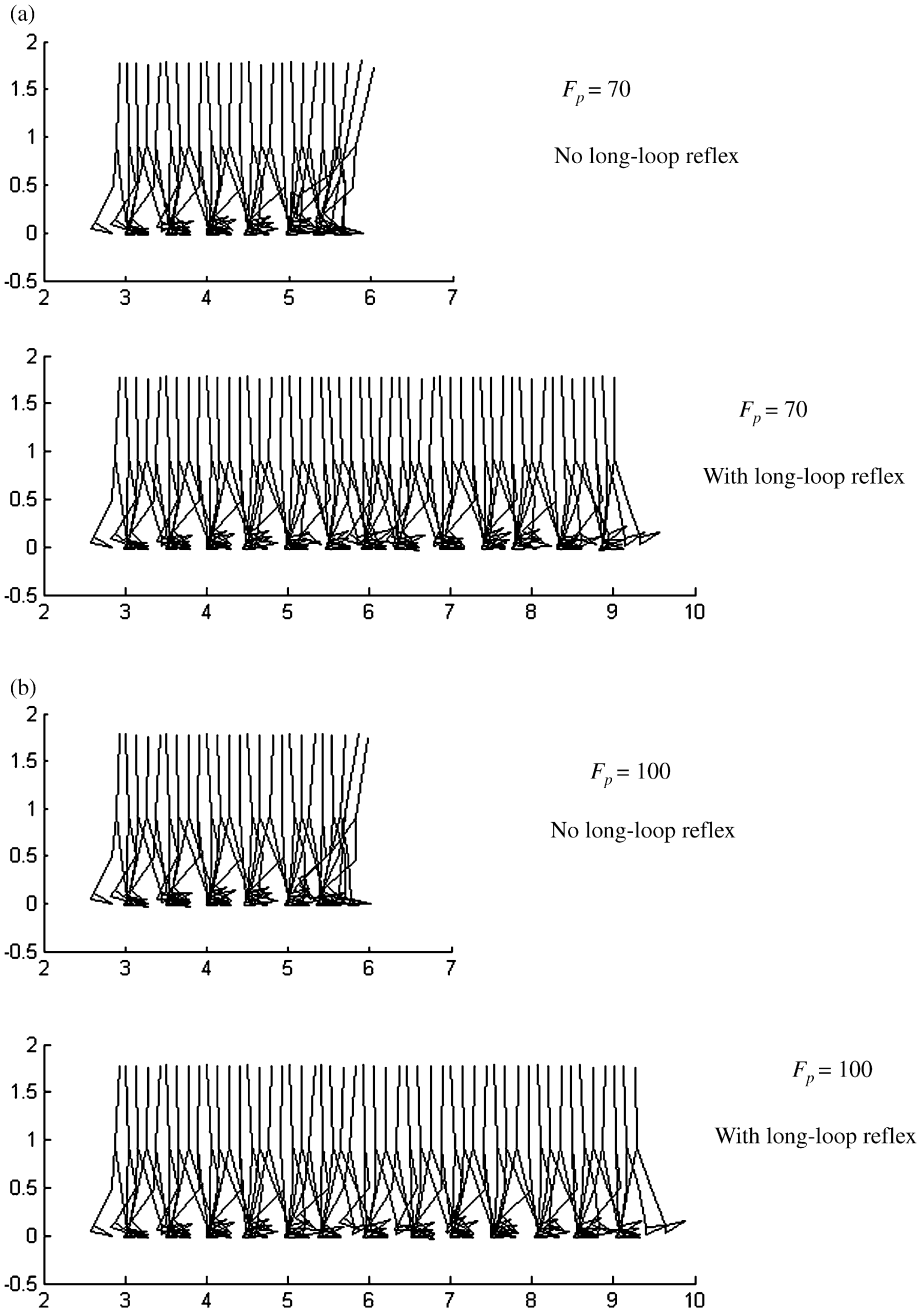

Fig. 13. The simulated walking behaviors with or without long-loop reflex through the cortex in the early swing perturbation (a) and the late swing perturbation (b).

As seen in Fig. 15, the perturbed leg contacts the ground earlier in the late swing perturbation, which is also shown in Fig. 15. The horizontal force accepting the body weight at heel-touch is smaller in the late swing perturbation. Ground interaction profiles in early swing perturbation are not much different from profiles before the perturbation evokes.

A tonic pulse from the cortex modulates the EMG responses against the perturbations. Fig. 16 demonstrates the simulated EMG patterns. Different recovery strategies are represented in different EMG patterns. Especially, ankle plantarflexor (right leg (6) in Fig. 16) activates in the lowering strategy, and ankle dorsiflexor (right leg (5) in Fig. 16) does in the elevating strategy (Schillings et al., 2000; Eng et al., 1994). Even though a tonic pulse descends, the muscular excitations around different joints evoke at different timings due to neural delays. After early swing perturbation, hip and knee flexors (right leg (1) and (3) in Fig. 16) activates further to implement the elevation strategy. The muscular activations in the stance leg (left leg) also change appropriately to maintain balance during the recovery behaviors.

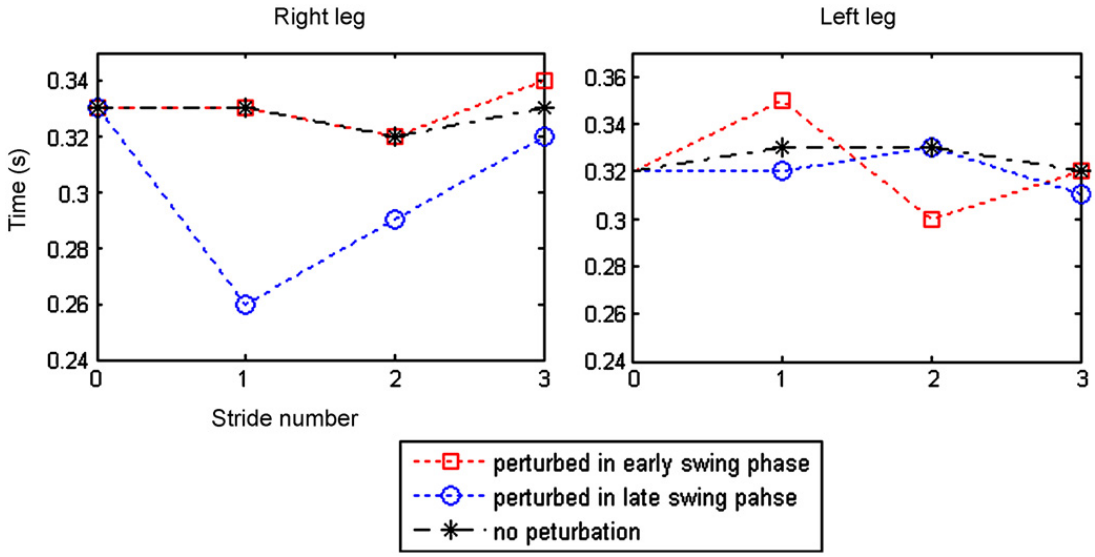

Fig. 14. The time intervals of the swing phase over gaits in both legs. Asterisks represent normal walking with no perturbation, boxes perturbed in early swing, and circles perturbed in late swing. Perturbation is applied to the right leg. Stride number 0 is before the perturbation and stride number 1 represents the perturbed phase and others subsequent strides represent the recovery.

4. Discussion

The human reaction strategies were computationally explained by phase resetting (Yamasaki et al., 2003) and gave an idea on preventing a humanoid walker from falling (Nakanishi et al., 2006). Prescribed joint trajectories were modified by resetting the phase against perturbation during gaits. The phase resetting achieved and was able to maintain stable walking. The humanoid walker's behavior is similar to either lowering or elevating strategy depending on whether the reset leads or lags in phase. According to the scheme, the recovery reaction enables implementation of phase resetting. In comparison with the phase resetting scheme, the model in this paper proposes a different neural principle for recovery behaviors. During nominal walking, the spinal pattern generator provides the basic feedforward neural command for normal walking pattern generation.

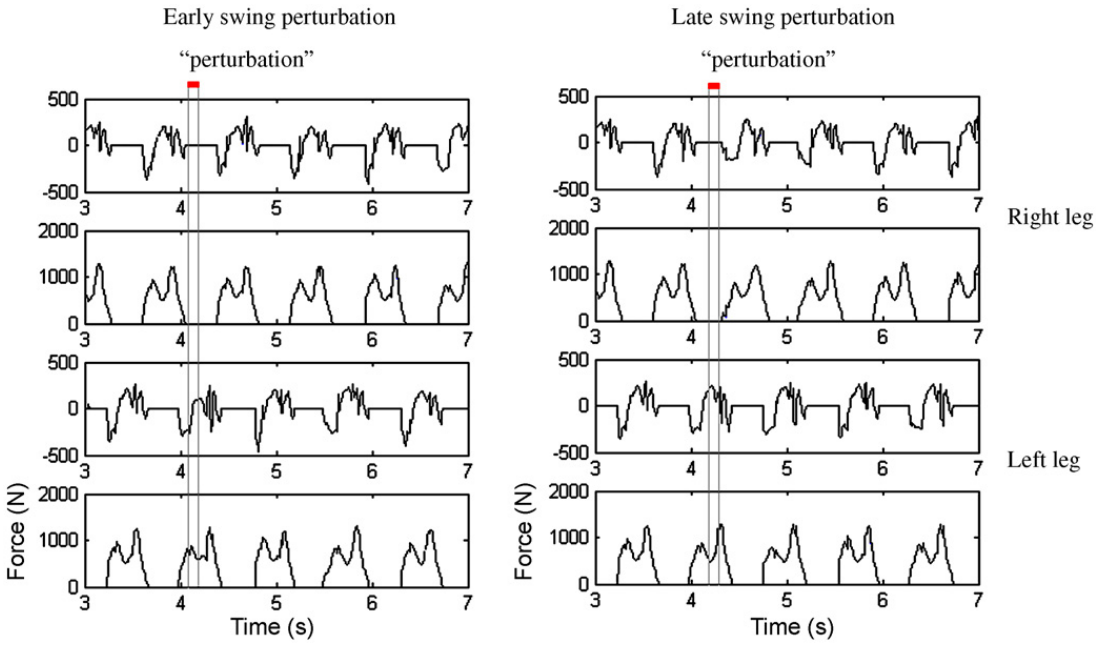

Fig. 15. The simulated ground interaction force profiles in the early swing perturbation (left) and the late swing perturbation (right). The top two rows indicate horizontal and vertical interaction forces in the right leg, and the bottom two rows in left leg. Right leg during the swing phase is perturbed.

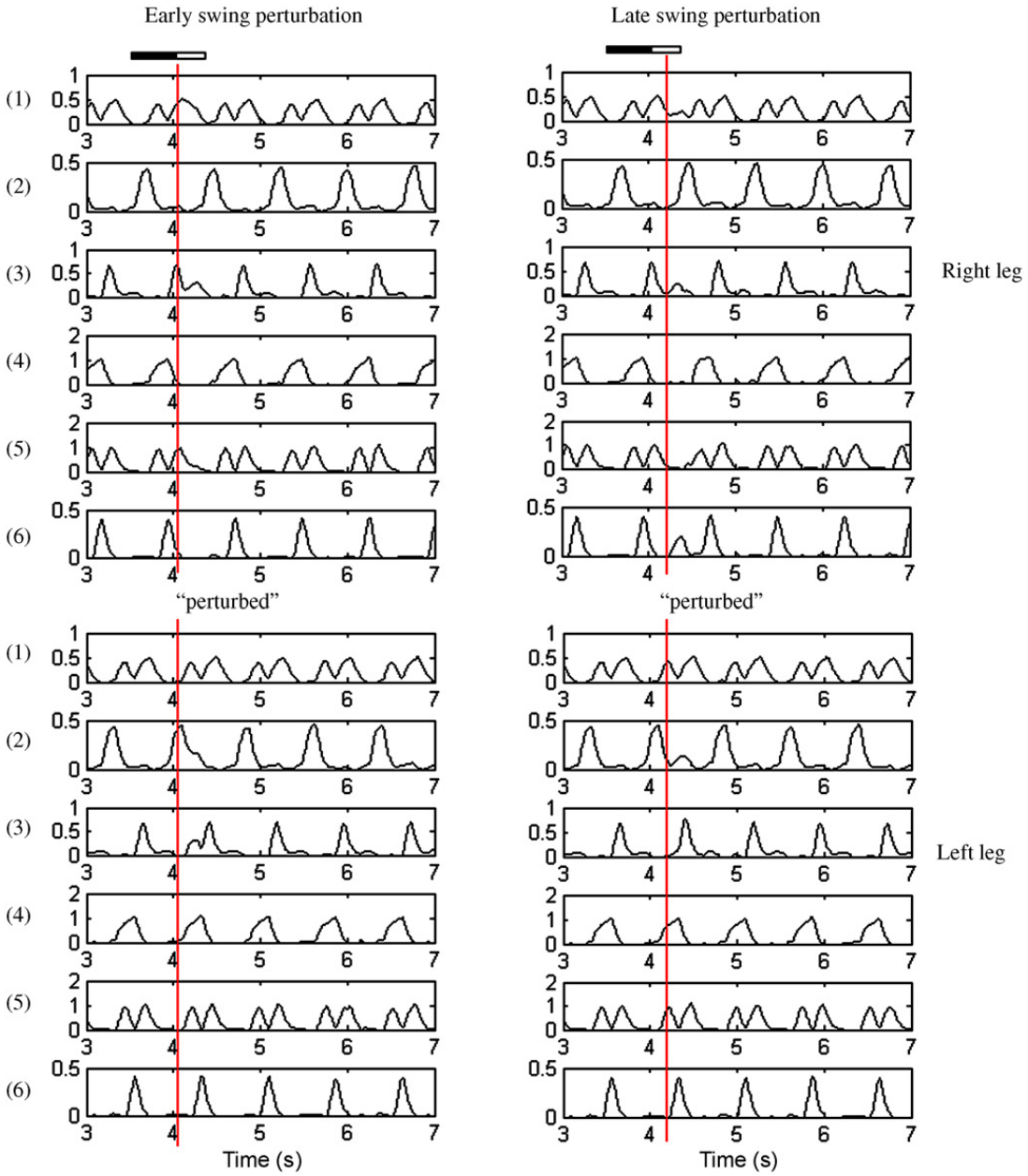

Fig. 16. The simulated EMG patterns of the early swing perturbation (left columns) and the late swing perturbation (right columns). (Top) The EMG patterns in the right leg; (bottom) the EMG patterns in the left leg. Vertical lines indicate the timings when perturbation evokes. A mini-bar indicates a gait cycle (filled black: stance, white: swing). Numbers in the left indicate the muscle groups in Fig. 1 (only monoarticular muscles are under consideration).

Whereas, the spinal reflex, vestibulo-spinal reflex, and supraspinal long-loop reflex modulate the neural patterns in a feedback manner. The hierarchical control system implements dynamically a stable limit cycle of walking when interacting with the environment. The long-loop supraspinal (cerebrocerebellar) feedback and spinal reflexes can maintain postural balance during normal walking or against small perturbations (Jo and Massaquoi, 2007) in a relatively monotonous manner. When a significant perturbation is detected, the feedforward pattern generator maintains the walking phase rather than explicitly resetting the phase. But a long-loop reflex through the cortex temporarily evokes the modification of neural activation so as to implement postural balance comparable with typical human recovery strategies. The long-loop reflex pathway is temporally triggered by the perturbation detection and, depending on the swing leg position (which also determines phase), different strategic recovery behaviors are selected. Different recovery behaviors are implemented by different neural control gains, which modulate different patterns of muscular activation.

A similar state-dependent control gain switching is argued in a previous study (Jo and Massaquoi, 2004). However, the verification of the neural mechanism remains unexplored. The recovery motion looks gait phase-dependent while gain selection is state-dependent. If the long-loop reflex control is evoked in the early swing phase, it will directly help stabilize the walking posture by controlling the swing leg and implement elevating strategy-type recovery. In the late swing perturbation, it turns out empirically that the model can stably recover normal walking motion after perturbation. This is accomplished even without the effect of the long-loop reflex up to a certain small magnitude of perturbation. In this case, the reflexes at the spinal cord level stabilize the walking posture influentially. However, the long-loop reflex helps realize rapid and more robust recovery behavior in the following steps. The simulation-based study demonstrates that lowering strategy-type recovery can be carried out by the long-loop reflex and can maintain stability against larger amounts of perturbation.

It is worthwhile to note that the proposed model does not generate detailed desired trajectories at the highest level of the motor system (i.e., planning). u_{ref} is simply constant. Furthermore, the spinal feedforward neural patterns are also rudimentary (rectangular). However, cooperative interaction among the neural systems creates appropriate activations to the muscles. The activation patterns play roles in the virtual equilibrium trajectories according to both lambda and alpha version of the equilibrium point control hypothesis (Bizzi et al., 1992). The equilibrium point control hypothesis suggests that the central nervous system commands a gradual transition of equilibrium points, which is the desired trajectory, without an explicit compensation for dynamics. The skeletal system controlled by spinal reflexes and muscles then generates a motion following the desired trajectory. From the perspective of the lambda version, the activation patterns play roles in desired trajectories. Then, the muscles (and spinal reflexes) act as the feedback control system about the desired trajectories and drive actual joint motions. From the perspective of the alpha version, the function of the activation patterns can be interpreted to modulate muscular stiffness or viscosity. The modulation of muscular viscoelasticity is substantially influential in enabling stable contact with the ground without explicit computation of joint torques or foot forces (Hogan, 1985). When postural recovery is necessary against a perturbation, the long-loop reflexes modify the activation patterns, i.e., virtual equilibrium trajectories, to incite a stable behavior against the perturbation. The whole integrated model in this study demonstrates concrete behaviors even with such a modification. The behavioral principle of the proposed model is comparable with the equilibrium point control hypothesis because the overall neural system of gait generation and strategic behavior-induction operates without seriously depending on body dynamics information.

Acknowledgements

I am grateful to the editor and reviewers for their valuable comments. I also thank Steve Massaquoi, Zhi-Hong Mao, Kazutaka Takahashi for many thought-provoking discussions, and Allen Atamer for his advice about my writing.

Appendix A

A.1. Simulation parameters

- *Musculo-skeletal model*: For simulation, total body mass: $m_{\mathrm{t}} = 80\,\mathrm{kg}$, total height: $h_{\mathrm{t}} = 1.8\,\mathrm{m}$; trunk, upper leg, lower leg, and foot masses are, respectively $0.678m_{\mathrm{t}}$, $0.1m_{\mathrm{t}}$, $0.047m_{\mathrm{t}}$, and $0.015m_{\mathrm{t}}$; their moments of inertia are, respectively $0.031m_{\mathrm{t}}h_{\mathrm{t}}^2$, $6.262 \times 10^{-4}m_{\mathrm{t}}h_{\mathrm{t}}^2$, $2.566 \times 10^{-4}m_{\mathrm{t}}h_{\mathrm{t}}^2$, and $4.976 \times 10^{-6}m_{\mathrm{t}}h_{\mathrm{t}}^2$; trunk, upper leg, and lower leg lengths are, respectively $0.47h_{\mathrm{t}}$, $0.245h_{\mathrm{t}}$, and $0.246h_{\mathrm{t}}$; foot is modeled as a triangle with height $0.039h_{\mathrm{t}}$ and length $0.152h_{\mathrm{t}}$; trunk, upper leg, and lower leg COM distances from lower end are, respectively $0.235h_{\mathrm{t}}$, $0.1389h_{\mathrm{t}}$, and $0.1395h_{\mathrm{t}}$; foot COM is located at $0.0195h_{\mathrm{t}}$ high from bottom and $0.0304h_{\mathrm{t}}$ ahead from heel. The estimations are determined based on Winter (1990).

  α, β, and γ are set to be 0.11, 0.4, and 0.6, respectively:

$$M = \begin{bmatrix} 0 & 0 & 0 & 0 & 0.023 & -0.036 & 0 & 0 & -0.040 \\ 0 & 0 & -0.040 & 0.049 & 0 & 0 & -0.025 & 0.049 & 0.050 \\ 0.132 & -0.092 & 0 & 0 & 0 & 0 & 0.049 & -0.054 & 0 \end{bmatrix}^{\mathrm{T}}$$

- *Ground interaction model*: $K_{gy} = 30{,}000$, $B_{gy} = 500$, $K_{gx} = 10{,}000$, $B_{gx} = 1000$; $\mu_k = 0.6$, $\mu_s = 1.2$.
- *Spinal pattern generator*: $f_{PG} = 1.3$, $s_{PG} = 1.2$; $\phi_1 = 0.38$, $\phi_2 = 1.2$, $\phi_3 = 0.705$, $\phi_4 = 0.5275$; $h_1 = 0.8763$, $h_2 = 0.8090$, $h_3 = 0.7501$, $h_4 = 0.9239$,

$$W_{PG} = \begin{bmatrix} 0.3 & 0 & 0 & 0.8 & 0.76 & 0 & 0 & 0 & 0 \\ 0 & 0.38 & 0 & 0 & 0 & 0 & 0 & 0 & 0 \\ 0.4 & 0 & 0.64 & 0 & 0 & 0 & 0 & 0 & 0 \\ 0 & 0 & 0 & 0.8 & 0.9 & 0.4 & 0 & 0 & 0 \end{bmatrix}^{T}$$

- *Spinal reflexes*:

$$W_v = [\,0.396 \quad -0.276 \quad 0 \quad 0 \quad 0 \quad 0 \quad 0.147 \quad -0.162 \quad 0\,]^{T},$$

$$q_0 = [\,0.35 \quad -0.35 \quad 0.55\,]^{T},$$

$$W = \rho \begin{bmatrix} 0 & 0 & 0 & 0 & 1 & 0 & 0 & 0 & 0 \\ 0 & 0 & 1 & 0 & 0 & 0 & 0 & 0 & 0 \\ 1 & 0 & 0 & 0 & 0 & 0 & 0 & 0 & 0 \end{bmatrix}^{T}$$

where ρ is a sufficient large number ($\rho > \eta_{PG}$).

$k_t = 0.5$, $k_r = k_f = 0.9$; $\delta_0 = 0.13$.

- *The cerebrocerebellar model*: $i_c = 0.2$, $f = 0.6$, $g_b = 0$, $g_k = 3$, $i_r = 100$, $p_{11} = 0.9663$, $p_{12} = 0.5343$, $p_{13} = 0.1414$; $p_{21} = 0.1405$, $p_{22} = 0.4416$, $p_{23} = -0.4416$, $W_{C,1} = [\,0 \quad 0 \quad 2 \quad -5 \quad 6 \quad -1 \quad 3 \quad -1 \quad -3\,]^{T}$, $W_{C,2} = [\,1 \quad -1 \quad -3 \quad 0 \quad 0 \quad 0 \quad 0 \quad 0 \quad 0\,]^{T}$,

$$W_{l,ES} = \left[\underbrace{\begin{matrix} 0.3 & 0 & 0.25 & 0 & 0.2 & 0 & 0 & 0 & 0 \end{matrix}}_{\text{muscles (1)–(9) of the right (perturbed) leg}} \; \underbrace{\begin{matrix} 0 & 0.15 & 0.35 & 0 & 0 & 0 & 0 & 0 & 0 \end{matrix}}_{\text{muscles (1)–(9) of the left leg}} \right]^{T},$$

$$W_{l,LS} = \left[\underbrace{\begin{matrix} 0.2 & 0 & 0.2 & 0 & 0 & 0.2 & 0 & 0 & 0 \end{matrix}}_{\text{muscles (1)–(9) of the right (perturbed) leg}} \; \underbrace{\begin{matrix} 0 & 0.1 & 0.2 & 0 & 0 & 0 & 0 & 0 & 0 \end{matrix}}_{\text{muscles (1)–(9) of the left leg}} \right]^{T}$$

where the threshold $x_T = -0.06$.

- *Initial conditions*: Joint angles: $\theta_1 = 0.2$, $\theta_3 = 0$, $\theta_5 = -0.2$ for right leg; $\theta_2 = 0$, $\theta_4 = -0.1$, $\theta_6 = 0.4$ for left leg. Angular velocities: $\dot{\theta}_1 = (f_{PG} + 1)/2$, $\dot{\theta}_3 = -(f_{PG} + 1)/2$, $\dot{\theta}_5 = (f_{PG} + 1)/2$ for right leg; $\dot{\theta}_2 = -(f_{PG} + 1)/2$, $\dot{\theta}_4 = (f_{PG} + 1)/2$, $\dot{\theta}_6 = -(f_{PG} + 1)/2$ for left leg.

References

Allen, G.I., Tsukahara, N., 1974. Cerebrocerebellar communication systems. Physiol. Rev. 54 (4), 957–1006.

Amstrong, D.M., Edgley, S.A., 1988. Discharges of interpositus and Purkinje cells of the cat cerebellum during locomotion under different conditions. J. Physiol. 400, 425–445.

Baxendale, R.H., Ferrell, W.R., 1981. The effect of knee joint afferent discharge on transmission in flexion reflex pathways in decerebrate cats. J. Physiol. (Lond.) 315, 231–242.

Bizzi, E., Hogan, N., Mussa-Ivaldi, F.A., Giszter, S.F., 1992. Does the nervous system use equilibrium-point control to guide single and multiple joint movements? Behav. Brain Sci. 15, 603–613.

Brand, R.A., Pedersen, D.R., Friderich, J.A., 1986. The sensitivity of muscle force predictions to changes in physiological cross-sectional area. J. Biomech. 8, 589–596.

Brooke, J.D., Cheng, J., Collins, D.F., McIlroy, W.E., Misiaszek, J.E., Staines, W.R., 1997. Sensori-sensory afferent conditioning with leg movement: gain control in spinal reflex and ascending paths. Prog. Neurobiol. 51, 393–421.

Calancie, B., Needham-Shropshire, B., Jacobs, P., Willer, K., Zych, G., Green, B.A., 1994. Involuntary stepping after chronic spinal cord injury: evidence for a central rhythm generator for locomotion in man. Brain 117, 1143–1159.

Christensen, L.O., Morita, H., Pertersen, N., Nielsen, J., 1999. Evidence suggesting that a transcortical reflex pathway contributes to cutaneous reflexes in the tibialis anterior muscle during walking in man. Exp. Brain Res. 124, 59–68.

Cordero, A.F., Koopman, H.J.F.M., van der Helm, F.C.T., 2004. Mechanical model of the recovery from stumbling. Biol. Cybern. 91, 212–220.

Cordero, A.F., Koopman, H.J.F.M., van der Helm, F.C.T., 2003. Multiple-step strategies to recover from stumbling perturbations. Gait Posture 18 (1), 47–59.

Dietz, V., Harkema, S.J., 2004. Locomotor activity in spinal cord-injured persons. J. Appl. Phsyiol. 96, 1954–1960.

Dimitrijevic, M.R., Gerasimenko, Y., Pinter, M.M., 1998. Evidence for a spinal central pattern generator in humans. Ann. NY Acad. Sci. 860, 360–376.

Duysens, J., Clarac, F., Cruse, H., 2000. Loading-regulating mechanisms in gait and posture: comparative aspects. Physiol. Rev. 80 (1), 83–133.

Eng, J.J., Winter, D.A., Patla, A.E., 1994. Strategies for recovery from a trip in early and late swing during human walking. Exp. Brain Res. 102, 339–349.

Flash, T., 1987. The control of hand equilibrium trajectories in multi-joint arm movements. Biol. Cybern. 57, 257–274.

Fujita, K., Sato, H., 1998. Intrinsic viscoelasticity of ankle joint during standing. In: Proceedings of the 20th annual conference of the IEEE engineering in medicine and biology society, vol. 20, no. 5, pp. 2343–2345.

Fuglevand, A.J., Winter, D.A., 1993. Models of recruitment and rate coding organization in motor-unit pools. J. Neurophysiol. 70 (6), 2470–2488.

Grasso, R., et al., 2004. Distributed plasticity of locomotor pattern generators in spinal cord injured patients. Brain 127 (5), 1019–1034.

Hogan, N., 1985. The mechanics of multi-joint posture and movement control. Biol. Cybern. 52 (5), 315–331.

Ito, M., 1997. Cerebellar microcomplexes. In: Schmahmann, J.D. (Ed.), The Cerebellum and Cognition, vol. 41. Academic, pp. 475–487.

Jo, S., Massaquoi, S.G., 2004. A model of cerebellum stabilized and scheduled hybrid long-loop control of upright balance. Biol. Cybern. 91 (3), 188–202.

Jo, S., Massaquoi, S.G., 2007. A model of cerebrocerebello-spinomuscular interaction in the sagitttal control of human walking. Biol. Cybern. 96 (3), 279–307.

Karameh, F.N., Massaquoi, S.G., 2005. A model of nonlinear motor cortical integration and its relation to movement speed profile control. In: Proceedings of the 27th annual conference of the IEEE-EMBS engineering in medicine and biology society, vol. 27, pp. 4331–4336.

Katayama, M., Kawato, M., 1993. Virtual trajectory and stiffness ellipse during multijoint arm movement predicted by neural inverse models. Biol. Cybern. 69, 353–362.

Lacquaniti, F., Soechting, J.F., 1986. Simulation studies on the control of posture and movement in a multi-jointed limb. Biol. Cybern. 54, 367–378.

Massaquoi, S.G., 1999. Modeling the function of the cerebellum in scheduled linear servo control of simple horizontal planar arm movements. PhD Thesis. Department of Electrical Engineering and Computer Science, MIT, Cambridge, MA, USA.

Massaquoi, S.G., Topka, H., 2002. Models of cerebellar function. In: Pandolfo, M., Manto, M. (Eds.), The cerebellum and its disorders. Cambridge University Press, Cambridge, pp. 69–94.

Mori, S., et al., 2004. Integration of multiple motor segments for the elaboration of locomotion: role of the fastigial nucleus of the cerebellum. Prog. Brain Res. 143, 341–351.

Nakanishi, M., Nomura, T., Sato, S., 2006. Stumbling with optimal phase reset during gait can prevent a humanoid from falling. Biol. Cybern. 95 (5), 503–515.

Nielsen, J.B., 2003. How we walk: central control of muscle activity during human walking. Neuroscientist 9 (3), 195–204.

Pijnappels, M., Bobbert, M.F., van Dieën, J.H., 2004. Control of support limb muscles in recovery after tripping in young and older subjects. Exp. Brain Res., 160.

Pijnappels, M., van Wezel, B.M.H., Colombo, G., Dietz, V., Duysens, J., 1998. Cortical facilitation of cutaneous reflexes in leg muscles during human gait. Brain Res. 787, 149–153.

Pinter, M.M., Dimitrijevic, M.R., 1999. Gait after spinal cord injury and the central pattern generator for locomotion. Spinal Cord 37, 531–537.

Rudomin, P., Schmidt, R.F., 1999. Presynaptic inhibition in the vertebrate spinal cord revisited. Exp. Brain Res. 129 (1), 1–37.

Schillings, A.M., van Wezel, B.M.H., Mulder, T.H., Duysen, J., 2000. Muscular responses and movement strategies during stumbling over obstacles. J. Neurophysiol. 83, 2093–2102.

Takahashi, K., 2006. Modeling cerebrocerebellar control in horizontal planar arm movements of humans and the monkey. PhD Thesis. Department of Aerospace and Aeronautic engineering, MIT, Cambridge, MA, USA.

Thach, W.T., Goodkin, H.P., Keating, J.G., 1992. The cerebellum and the adaptive coordination of movement. Annu. Rev. Neurosci. 15, 403–442.

Vogelstein, R.J., Etienne-Cummings, R., Thankor, N.V., Cohen, A.H., 2006. Phase-dependent effects of spinal cord stimulation on locomotor activity. IEEE Trans. Neural Syst. Rehabil. Eng. 14 (2), 257–265.

Winter, D.A., 1990. Biomechanics and Motor Control of Human Movement. Wiley, New York.

Yamasaki, T., Nomura, T., Sato, S., 2003. Phase reset and dynamic stability during human gait. Biosystems 71, 221–232.

Zehr, E.P., Stein, R.B., 1999. What functions do reflexes serve during human locomotion? Prog. Neurobiol. 58, 185–205.